The Influence of Sulphur Content on the Carbothermal Reduction of SiMn Slag

Xiang Li [a,b]✉*, Merete Tangstad [b]

[a] School of Energy and Power Engineering, Jiangsu University, Jiangsu 212013, China

[b] Department of Materials Science and Engineering, Norwegian University of Science and Technology, 7491 Trondheim, Norway

Abstract

This article examines the influence of sulphur content on the carbothermal reduction of MnO and SiO_2 in SiMn slag by carbon black. The sulphur content in the synthetic slag is varied from 0 to 1.0 wt pct. Reduction experiments are carried out in a thermo-gravimetric (TG) furnace at 1873 K (1600 °C) under CO atmospheric pressure. The reduction rates are measured based on the weight loss data, and the samples are characterized by SEM/EDS and ICP-MS. The wetting property of slag on carbon black is also studied with the sessile drop technique. The reaction rate on the slag-metal interface is one order higher than on the slag-carbon interface. A small amount of sulphur (0.2 wt pct and 0.44 wt pct) accelerates the slag-metal reaction rate constant by 2.2 times and 4.2 times, respectively. Therefore, small amounts of sulphur in slag significantly improve the reduction of MnO and SiO_2. The MnS precipitation phenomenon during slag cooling is studied by FactSage simulation and experimental verification.

* Corresponding author, email: xiangli@ujs.edu.cn Tel: +86 15751012916

Keywords: Metallurgy; SiMn slag; Sulphur; Reaction kinetics; MnS

1. Introduction

The industrial production of silicomanganese (SiMn) alloys involves the simultaneous carbothermal reduction of MnO and SiO_2 dissolved in a liquid slag at high temperatures of 1773–1923 K (1500–1650 °C) [1, 2]. The dominating components of the SiMn slag are MnO, SiO_2, Al_2O_3, CaO and MgO. MnO and SiO_2 are reduced into a molten alloy solution either by solid carbon in coke or by carbon dissolved in metal according to the following reactions [3, 4]:

$$MnO\ (l) + C\ (s, l) = Mn\ (l) + CO\ (g) \quad (1)$$

$$SiO_2\ (l) + 2\ C\ (s,l) = Si\ (l) + 2\ CO\ (g) \quad (2)$$

In recent decades, the kinetics of MnO reduction in the field of ferromanganese (FeMn) production processes, where solid MnO still exists, have been studied extensively [5-8]. In this process, the activity of MnO is hence much higher than in SiMn slag [5–8]. It has been observed that stirring has no effect on the kinetics of MnO reduction, while the reduction rate is highly sensitive to temperature. Therefore, it has been concluded that MnO reaction kinetics are not controlled by any transport mechanism but are controlled by chemical reaction [5, 6]. The rate and extent of MnO reduction are affected by the slag chemistry, including concentrations of different oxides and trace elements. In a homogenous liquid slag, higher basicity was found to produce a higher reduction rate of MnO [6–8]. This finding could be due to the higher driving force given by the effect of CaO and MgO on the activity of MnO or by the effect these oxides have on the viscosity of the

slag. SiO_2 reduction is more difficult than MnO reduction and requires higher temperatures. While MnO is reduced by both solid carbon and dissolved carbon in metal, the formation of Si requires a metal phase with low Si activity [1]. A linear relationship between the activity of SiO_2 in the slag and the reduction rate was reported by several investigations, indicating that its kinetics are also controlled by the interfacial chemical reaction [9–11].

Some trace elements in carbon and ore are known to have important effects on reduction rates as catalysts. The sulphur content is of particular interest. Sulphur is known as a surface-active element and significantly decreases the surface tension of the liquid iron on refractories [12–15]. Xu et al. [6, 16] observed that the rate of MnO reduction by carbon-saturated iron is decreased with the increase in sulphur content from 0.027 wt pct to 0.079 wt pct. It was explained that the effective reaction area decreases due to the adsorption of sulphur in the slag-metal boundary layer. In contrast, other researchers reported a positive effect of small amounts of sulphur on the MnO reduction rate. Skjervheim et al. [8, 17] found that industrial slags are reduced 5 to 10 times faster than synthetic slags with apparently the same composition due to increased sulphur content. The reduction rate of synthetic slag is considerably increased if 0.2 wt pct S is added to the system. Recently, Larssen [18] and Kim [19] also reported similar results for SiMn slag with less than 0.4 wt pct S. Some researchers found that excess sulphur content in the slag (≥1.0 wt pct) seems to retard the reduction of MnO without a reliable explanation [20, 21].

This study investigates the carbothermal reduction of SiMn slag by carbon black at 1873 K (1600 °C) in CO atmosphere. The slags are synthesized with different sulphur contents. The aim

of this article is to establish the effects of sulphur content in slag on the rate and mechanisms of MnO and SiO_2 reduction.

2. Experiment

2.1 Reduction of SiMn slag by carbon black

The SiMn slag used in this study is synthetic slag with initial compositions of a CaO/MgO weight ratio of 2.5 and a (CaO+MgO)/Al_2O_3 weight ratio of 1.0. Fine powders of MnO (VWR International, 99.5 pct), SiO_2 (VWR International, 99.5 pct), CaO (Sigma-Aldrich, 99.0 pct), MgO (Sigma-Aldrich, 98.0 pct), Al_2O_3 (Sigma-Aldrich, 99.0 pct) and FeS (VWR International, 99.9 pct) are used for the synthesis of SiMn slag with different sulphur contents. The powders are weighed and mixed in a plastic jar with zirconia balls for 2 hours. Then, the mixture is transferred to a molybdenum crucible and melted at 1673 K (1400 °C) for 20 min with an induction furnace in an Ar atmosphere. After cooling in the furnace, the slag is crushed and sieved to different size ranges. A slag sample without sulphur is RM-1. Slag samples with sulphur of 0.2 wt pct, 0.44 wt pct and 1.0 wt pct are RM-2, RM-3 and RM-4, respectively. The compositions of synthetic slags are presented in Table I. The oxide compositions of slag are analysed by EDS mapping, and the sulphur content is analysed by ICP-MS. The synthetic slags after melting at 1400 °C consist of two different phases, as shown in Figure 1. The bright area is the olivine ((Ca,Mg,Mn)O.SiO_2) phase, and the dark area is the glass matrix. Since the distribution of the olivine phase is uniform in all slags, we apply EDS mapping several times at each slag and calculate the average slag compositions.

Table I. Chemical compositions (wt pct) of synthetic slags analysed by EDS mapping and sulphur content (wt pct) analysed by ICP-MS.

Slag No.	S adding	MnO	SiO_2	CaO	MgO	Al_2O_3	FeO	Total*	S by analyse
RM-1	0	40.2	33.4	9.3	3.7	13.0	0.0	99.6	0.01
RM-2	0.20	40.0	33.4	9.4	3.6	12.9	0.6	99.9	0.20
RM-3	0.44	39.7	33.2	9.3	3.7	12.9	1.1	99.9	0.39
RM-4	1.0	39.0	32.6	9.1	3.6	12.7	2.2	99.3	0.86

* Total wt pct = MnO wt pct + SiO_2 wt pct + CaO wt pct + MgO wt pct + Al_2O_3 wt pct + FeO wt pct

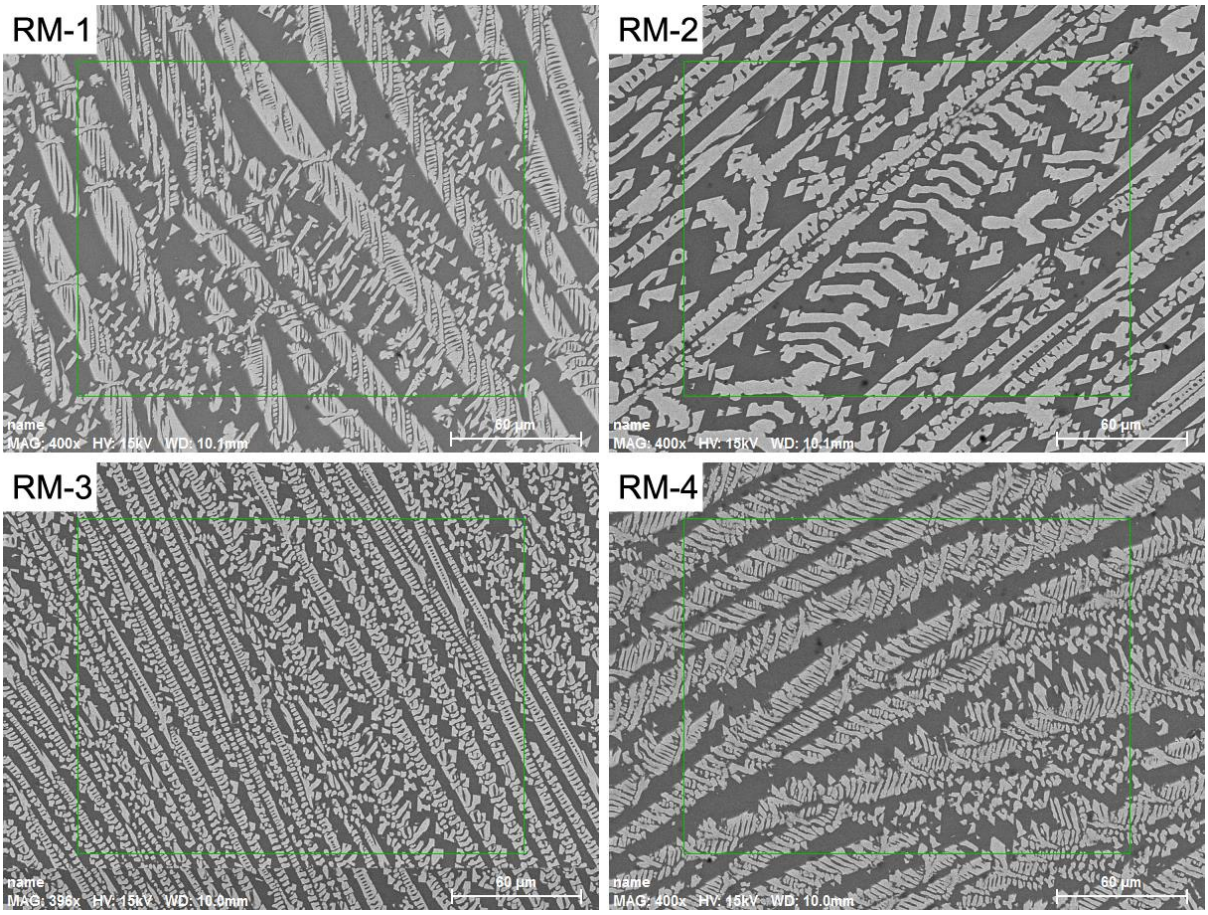

Fig. 1–The images of synthetic slags RM-1, RM-2, RM-3 and RM-4 taken during EDS mapping.

The carbon material used in this study is carbon black (Cancarb Limited, Thermax® N990 Ultra Pure). The properties of carbon black listed in Table II are supplied by Cancarb Limited. CO and Ar gas with purity of 99.999 pct are supplied by AGA industrigasser AS (Oslo, Norway) in 50-litre gas cylinders.

Table II. Properties of carbon black.

Average particle size (μm)	BET surface area (m^2/g)	Ash content (wt pct)	S content (wt pct)
1.2	9.4	0.02	0.006

Reduction experiments are carried out in a laboratory vertical graphite tube furnace equipped with thermo-gravimetric (TG) balance, as shown in Figure 2. Typically, 10 g of slag (with particle size range of 0.5~1.25 mm) and 2.5 g of carbon black powder are weighed into a graphite crucible with an inner diameter of 30 mm and depth of 61 mm. Slag and carbon are mixed well in the crucible by stirring. The crucible with a lid is suspended by a molybdenum wire to the balance and positioned in the hot zone of the furnace. The crucible temperature is measured by a type B thermocouple, which is approx. 0.5 cm away from the bottom of the crucible. During the reduction, the CO flow rate is fixed to 0.5 Nl/min. The furnace is heated to 1523 K (1250 °C) with a heating rate of 25 K/min, where it is kept for 30 min. Then, the furnace is heated to 1873 K (1600 °C) at a heating rate of 10 K/min and kept for 60 min. The weight loss of a sample is recorded every 5 seconds. After finishing the experiment, the reduced sample is weighed and subjected to further characterization.

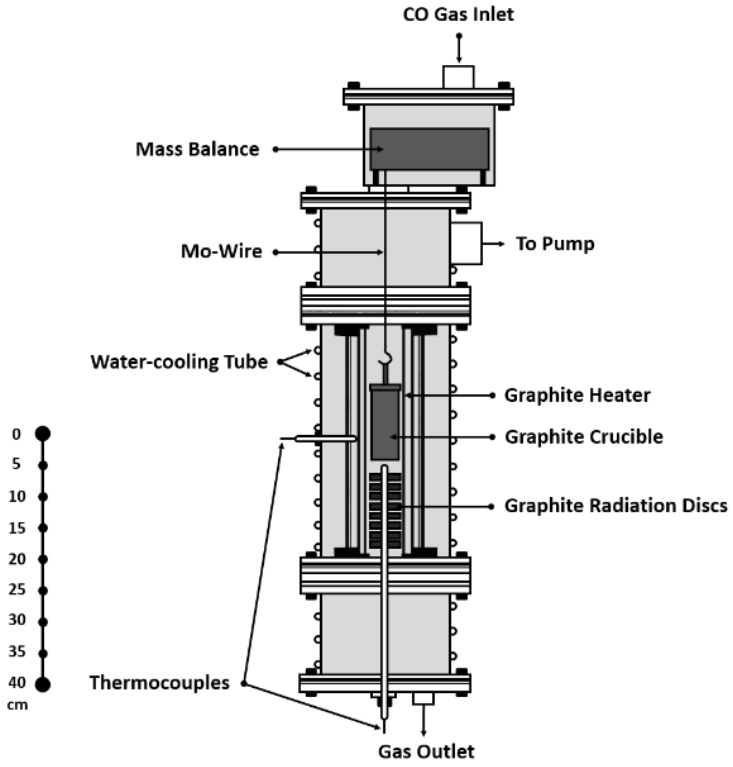

Fig. 2–Schematics of the thermo-gravimetric (TG) furnace, reprinted from Ref. [22].

2.2 Wetting property of slag

Slag's wetting property on carbon black substrates is also studied. The carbon black powder is pressed into substrate with a diameter of 10 mm with an aerostatic press under 63.7 kg/cm^2 pressure. A horizontal tube furnace is used to study the wetting properties with the sessile drop method. Figure 3 shows the furnace with the element in the centre, and the sample holder sitting in the middle of the furnace is normally mounted to the left and the camera lens to the right. The carbon substrate is located in the graphite holder, and a slag particle (approx. 40 mg) is placed on the substrate. During the experiment, the CO gas flow rate is kept at 0.5 Nl/min. The furnace temperature is controlled by a Keller PZ40 two-colour pyrometer operating from 900 to 2400 ˚C and focused on the graphite sample holder. A type C thermocouple is also involved to measure the

temperature under 2273 K (2000 ˚C). The sample is heated to 1223 K (950 ˚C) with a rapid heating rate of 300 K/min and followed with a heating rate of 50 K/min to 1473 K (1200 °C) and then 10 K/min to 1873 K (1600 ˚C). A fire-wire digital video camera (Sony XCD-SX910CR) with a telecentric lens (Navitar 1-50993D) is used to record images from the sample at 960×1280 pixels. In the experiment, images are captured every 0.5 seconds. The contact angles between slag drop and substrate are measured directly from the image of the drop using Video Drop Shape Analysis software (First Ten Angstroms, Inc., Portsmouth, VA).

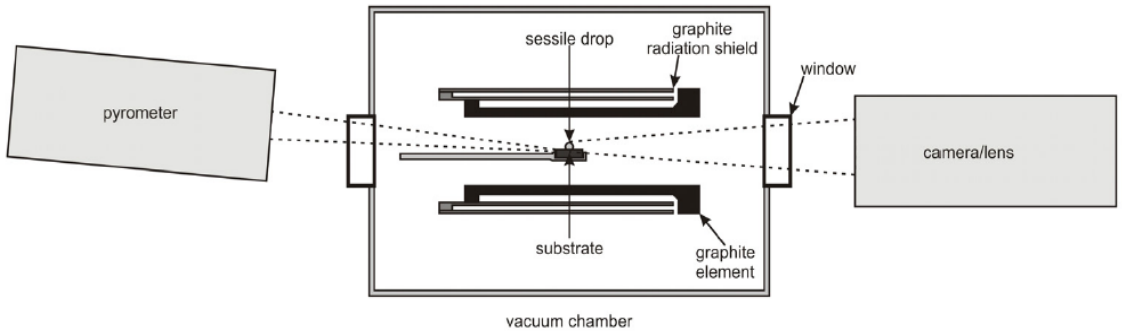

Fig. 3–Sessile drop experimental setup, reprinted from Ref. [23].

2.3 Slag-carbon and slag-metal interface reactivity

Eight experiments are carried out in a TG furnace to calculate the influence of sulphur content on the slag-carbon and slag-metal interface reaction rates. A schematic view of the experimental setup is shown in Figure 4, and the experimental conditions are summarized in Table III. In all experiments, 40 g of manganese chips (Sigma-Aldrich, 99.0 pct) is first weighed in a graphite crucible (inner diameter 30 mm, deep 61 mm) and melted at 1673 K (1400 °C) for 20 min in the atmosphere of Ar. In the MC-1, MC-3, MC-5 and MC-7 experiments, a layer of Mo sheet with

146 0.15 mm thickness is inserted into the crucibles with melted metal to cover the slag from the
147 graphite crucible wall. Hence, the reaction between the slag and graphite crucible is stopped. In
148 MC-2, MC-4, MC-6 and MC-8 experiments, no Mo sheet is used, and the graphite crucible will
149 also be a reductant. Twenty-five grams of slag powder is added to the crucible. The crucible is
150 heated to 1523 K (1250 °C) in the TG furnace at a heating rate of 20 K/min, then to 1873 K
151 (1600 °C) with a heating rate of 10 K/min and then maintained for 30 min. The gas atmosphere is
152 CO with a gas flow rate of 0.5 NL/min. The sample weight loss is recorded every 5 seconds.
153

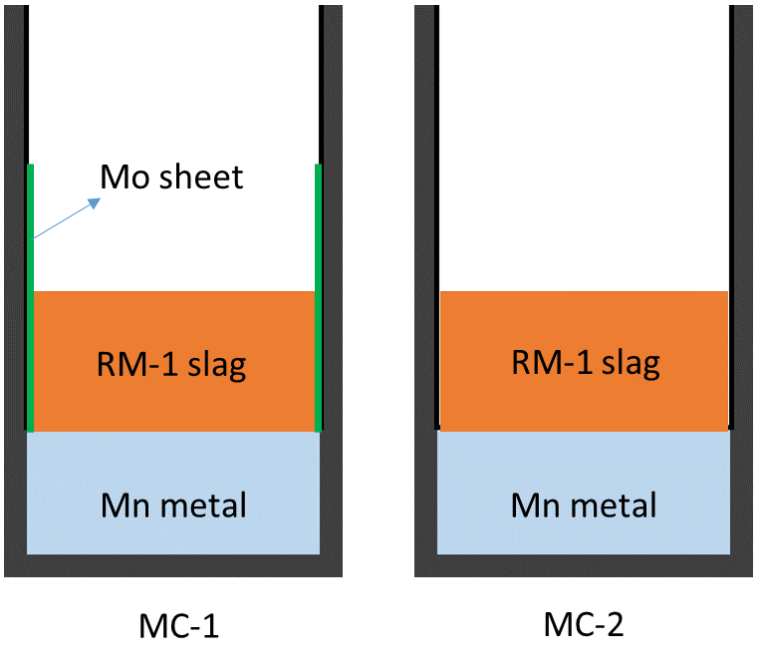

154
155 Fig. 4–The schematic view of the experimental setup for slag-carbon and slag-metal interface
156 reaction rate testing.
157
158
159

Table III. Experimental conditions for interface reaction rate testing.

Exp. no.	Slag	Slag (g)	Metal	Metal (g)	Temperature (K)	Crucible type
MC-1	RM-1	25	Mn	40	1873	Graphite crucible with Mo wall
MC-2	RM-1	25	Mn	40	1873	Graphite crucible
MC-3	RM-2	25	Mn	40	1873	Graphite crucible with Mo wall
MC-4	RM-2	25	Mn	40	1873	Graphite crucible
MC-5	RM-3	25	Mn	40	1873	Graphite crucible with Mo wall
MC-6	RM-3	25	Mn	40	1873	Graphite crucible
MC-7	RM-4	25	Mn	40	1873	Graphite crucible with Mo wall
MC-8	RM-4	25	Mn	40	1873	Graphite crucible

2.4 Sample characterization

The crucibles containing reacted slag are casted using Epoxy resin and then cut to expose the slag and metal. The samples are ground and carefully polished and coated with carbon film to enhance conductivity during SEM/EDS observation. SEM images are recorded by field-emission scanning electron microscopy (FESEM, Zeiss Ultra 55 LE, Oberkochen, Germany) operated at 15 KV. The chemical composition of the slag is analysed by energy-dispersive X-ray spectrometer (EDS) point or mapping analysis.

The sulphur content in the slag sample is determined by inductively coupled plasma mass spectrometry (ICP-MS) (Agilent 8800, Santa Clara, United States). Before analysis, approximately

30 mg of sample powder was weighed and dissolved in a 1.5 HNO_3 + 0.5 HF acid mixture. Then, the liquid is diluted to 216 ml with de-ionized water in a calibrated flask. Blank samples are prepared in a similar manner to monitor contamination during the entire analytical process. Each sample is analysed three times for multiple replicates, and the average results are calculated.

2.5 Thermodynamic calculations

In this study, the activity of MnO in the slag (a_{MnO}), the activity of SiO_2 in the slag (a_{SiO_2}), the activity of Mn in the metal (a_{Mn}) and the activity of Si in the metal (a_{Si}) are calculated by Eq. (3), Eq. (4), Eq. (5) and Eq. (6), respectively. These equations are obtained by activity data collection from FactSage 7.0 software [24] and linear fitting [25].

$$a_{MnO} = C_{MnO} \cdot \exp(0.0007576T - 123.7C_{MnO} + 30.14C_{SiO_2} + 47.84C_{MgO} + 49.54C_{CaO} - 47.96C_{Al_2O_3} + 122.8C_{MnO}^2 - 67.78C_{SiO_2}^2 - 46.32C_{MgO}^2 - 47.68C_{CaO}^2 + 22.51C_{Al_2O_3}^2 + 78.35C_{MnO}C_{CaO} + 77.56C_{MnO}C_{MgO} + 176.6C_{MnO}C_{Al_2O_3} + 101.2C_{MnO}C_{SiO_2} - 71.52C_{SiO_2}C_{CaO} - 70.58C_{SiO_2}C_{MgO} + 27.35C_{SiO_2}C_{Al_2O_3} + 46C_{SiO_2}^3 - 92.97C_{CaO}C_{MgO} + 2.44C_{CaO}^3) \quad (3)$$

$$a_{SiO_2} = C_{SiO_2} \cdot \exp(-0.0003408T + 113.8C_{MnO} - 22.79C_{SiO_2} - 51.63C_{MgO} - 52.44C_{CaO} + 36.3C_{Al_2O_3} - 119.3C_{MnO}^2 + 42.56C_{SiO_2}^2 + 32.25C_{MgO}^2 + 30.12C_{CaO}^2 - 26.26C_{Al_2O_3}^2 - 82.725C_{MnO}C_{CaO} - 82.9C_{MnO}C_{MgO} - 155.2C_{MnO}C_{Al_2O_3} - 86.98C_{MnO}C_{SiO_2} + 86.21C_{SiO_2}C_{CaO} + 86.19C_{SiO_2}C_{MgO} - 23.06C_{SiO_2}C_{Al_2O_3} - 31.26C_{SiO_2}^3 + 69.45C_{CaO}C_{MgO} + 11.29C_{CaO}^3) \quad (4)$$

$$a_{Mn} = C_{Mn} \cdot \exp(0.0005382T - 37.41C_{Mn} - 2.966C_{Si} - 0.6835C_{Fe} + 39.52C_{Mn}^2 - 1.453C_{Si}^2 - 0.5561C_{Fe}^2 + 27.48C_{Mn}C_{Si} + 38.69C_{Mn}C_{Fe} + 0.214C_{Si}C_{Fe}) \quad (5)$$

$$a_{Si} = C_{Si} \cdot \exp(0.002464T + 10.3C_{Mn} - 1.081C_{Si} + 27.52C_{Fe} - 15.49C_{Mn}^2 - 3.713C_{Si}^2 - 34.66C_{Fe}^2 + 1.324C_{Mn}C_{Si} - 47.01C_{Mn}C_{Fe} - 9.127C_{Si}C_{Fe}) \quad (6)$$

where $C_{MnO}, C_{SiO_2}, C_{CaO}, C_{MgO}, and\ C_{Al_2O_3}$ are the mass fractions of MnO, SiO_2, CaO, MgO, and Al_2O_3 in the slag phase, and $C_{Mn}, C_{Si}, C_{Fe}, and\ C_C$ are the mass fractions of Mn, Si, Fe, and C in the metal phase, respectively.

3. Results

3.1 Reduction of SiMn slag by carbon black

Reduction of SiMn slag with different sulphur contents is carried out in a TG furnace in a CO atmosphere. The weight loss versus time for different charges is presented in Figure 5, and the temperature profile is also shown. The temperature rapidly increases to 1523 K (1250 °C) and is held for 30 min to ensure the completion of slag melting and prereduction of Fe^{2+}, which is called the prereduction stage, as described by Reactions (7), (8) and (9). Other metal cations M^{i+} (Mn^{2+}, Ca^{2+}, Mg^{2+}, Al^{3+}, Si^{4+}) have greater ionic bonding characteristics for S^{2-} than Fe^{2+} [26].

$$FeS = Fe^{2+} + S^{2-} \quad (7)$$

$$MO_{0.5i} = M^{i+} + 0.5iO^{2-} \quad (8)$$

$$Fe^{2+} + CO(g) + O^{2-} = Fe(l) + CO_2(g) \quad (9)$$

Subsequently, the temperature increases to 1873 K (1600 °C) and is held for 60 min. The weight loss is not visibly different between different slags at temperatures below 1873 K (1600 °C). However, in the isothermal stage, slag samples with sulphur show faster reduction rates than RM-1. The final weight loss of RM-1 is 1.44 g. It increases to 1.84 g with 0.2 wt pct S and 2.55 g with 0.44 wt pct S. However, RM-4 slag with 1.0 wt pct S shows the opposite trend, and its final weight loss decreases to 2.33 g. The weight loss curves indicate that sulphur increases the reduction rate, and there is an optimal sulphur content.

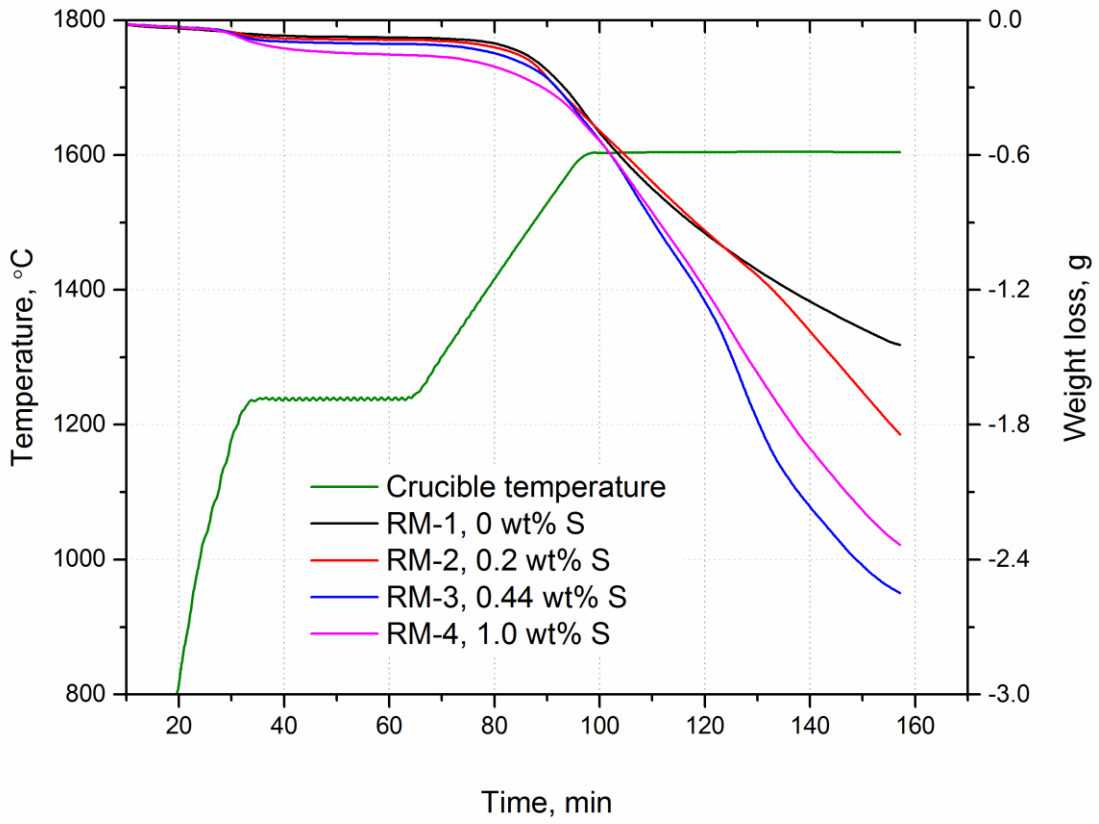

Fig. 5–Temperature profile and thermogravimetric curves for experiments with different sulphur contents in slag using carbon black as the reductant.

The slag composition is measured by EDS point analysis. Each slag sample is analysed at least 6 times at different spots, and the slag compositions are summarized in Table IV. The MnO content drops to 11.5 wt pct when the initial sulphur content is 0.44 wt pct and increases to 14.9 wt pct with more sulphur (1.0 wt pct) in the slag. However, the SiO_2 content shows insignificant changes with the increase in sulphur content.

Table IV. Chemical compositions of slag samples after reduction, analysed by EDS.

Slag No.	S adding (wt pct)	MnO (wt pct)	SiO_2 (wt pct)	CaO (wt pct)	MgO (wt pct)	Al_2O_3 (wt pct)	Total (wt pct)
RM-1	0	31.2	36.6	11.4	4.8	16.0	100.0
RM-2	0.20	20.2	39.7	14.3	5.8	20.1	100.0
RM-3	0.44	11.5	40.2	17.1	7.00	24.3	100.0
RM-4	1.0	14.9	39.7	16.3	6.5	22.6	100.0

The calculated metal produced and composition based on slag compositions are presented in Table V. It is assumed that the total amount of CaO, MgO and Al_2O_3 in the slag is constant before and after reduction. The metal produced also has a similar trend with final weight loss in Figure 5. The metal produced in RM-3 is more than double RM-1. The Mn content in metal decreases with the increase in sulphur content due to the increase in Si and Fe contents. It is interesting to note that the calculated data are usually more reliable than measured metal compositions by EDS, as the produced metal phase always randomly separates into two phases during solidification, as shown in Figure 6. The bright phase is the $(Mn,Fe)_{33}Si_7$ phase, and the dark phase is the $(Mn,Fe)_5Si_3$ phase, as shown in the Mn-Si phase diagram.

Table V. Calculated metal produced and metal compositions after reduction.

Slag No.	S adding (wt pct)	Metal produced (g)	Composition (wt pct)			
			Mn	Si	Fe	Total
RM-1	0	1.33	86.4	13.6	0	100.0
RM-2	0.20	2.49	84.1	14.5	1.5	100.0
RM-3	0.44	3.27	80.6	16.9	2.5	100.0
RM-4	1.0	3.14	78.0	16.0	6.1	100.0

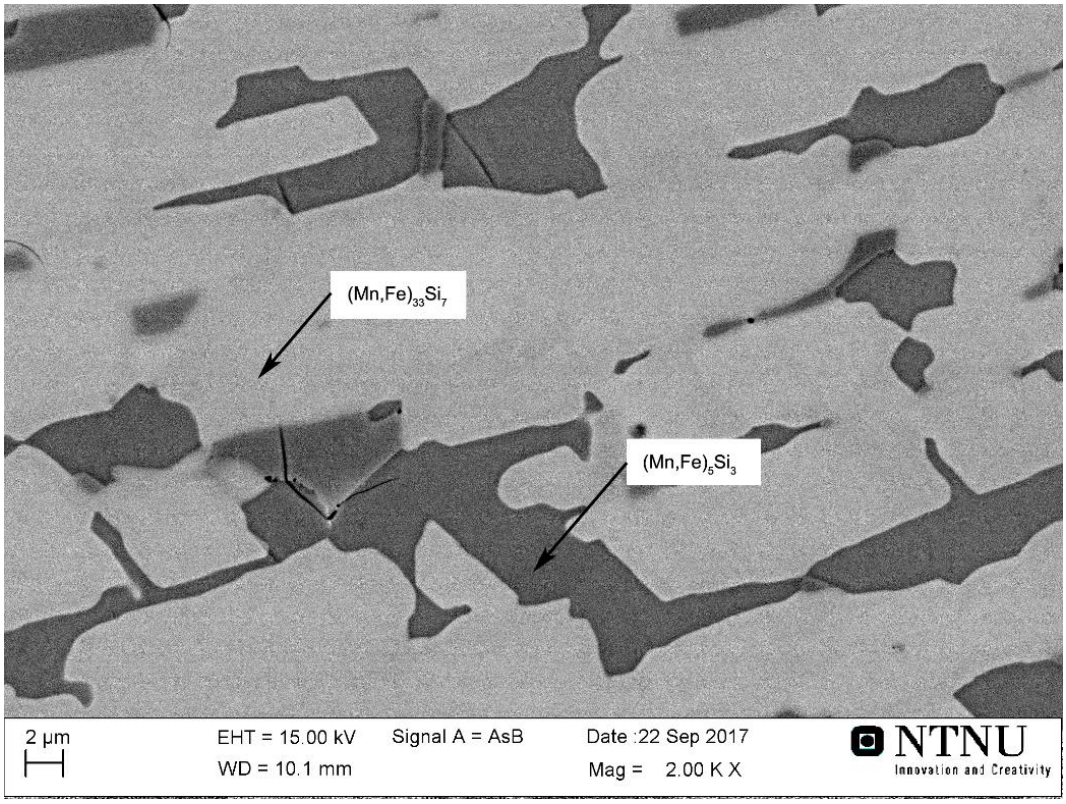

Fig. 6–The image of the metal phase of RM-3 after reduction.

Figure 7 presents the SEM images of RM-1 and RM-2 slag samples collected after reduction at 1873 K (1600 °C) with 1000x magnification. Both of them contain some metal drops in the slag matrix confirmed by EDS point analysis. The SEM images of RM-3 slag after reduction are shown in Figure 8. Figure 8(a) contains three different bright phases, including metal drops shown in Figure 8(b), MnS precipitation prills shown in Figure 8(c), and MnS precipitation dendrites shown in Figure 8(d). EDS mapping results from Figure 8(b) are shown in Figure 9 and indicate that the metal drop mainly contains Mn, Fe and Si, and there is MnS precipitation on its outer layer. RM-4 slag also contains a large amount of MnS precipitation phase, as shown in Figure 10(a). It appears that their sizes are larger in RM-4 than in RM-3 slag, as shown in Figures 10(b) and 10(c), respectively. The MnS phase is believed to be precipitated during cooling, and this finding will be further discussed in Section 4.1.

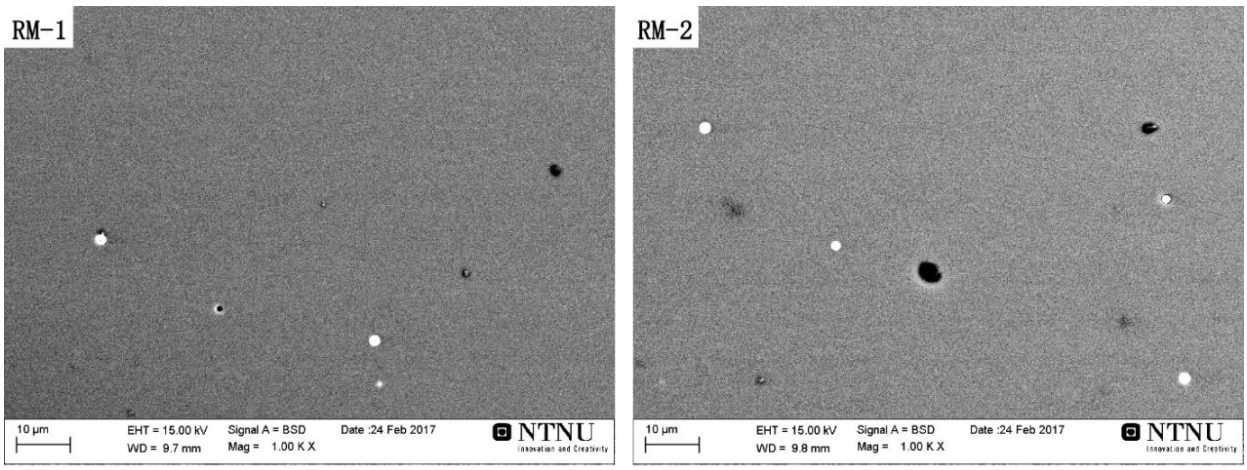

Fig. 7–The images of RM-1 and RM-2 slag after reduction.

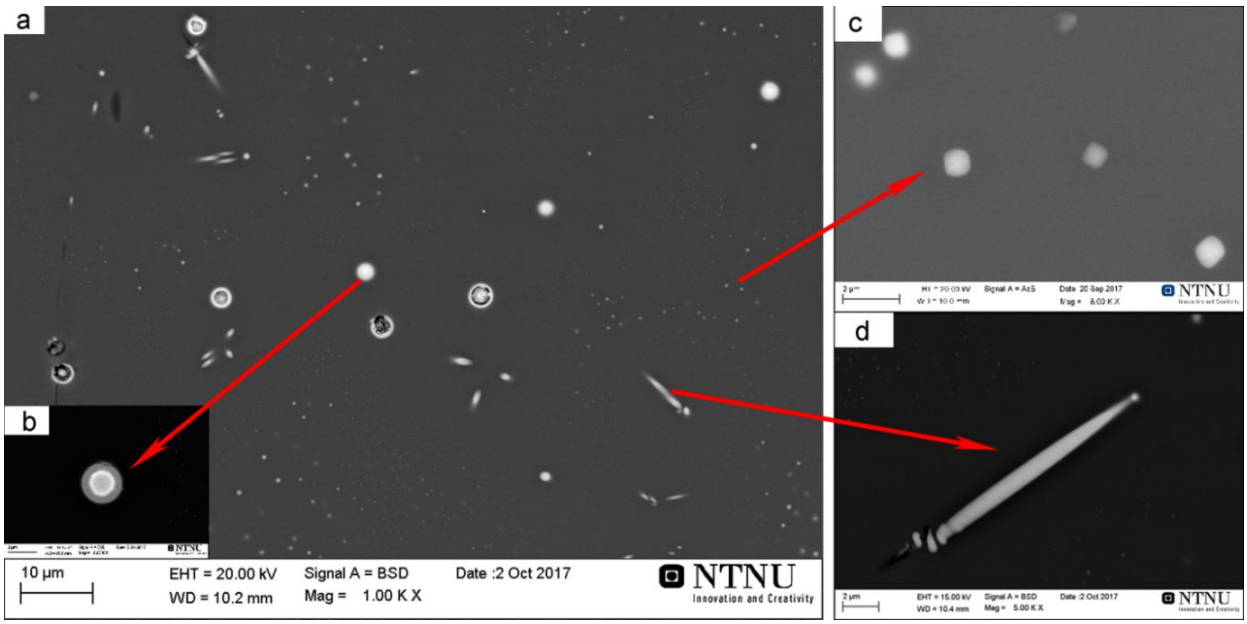

Fig. 8–The images of RM-3 slag after reduction. (a) Image with 1000x magnification; (b) image of metal drop with MnS outer layer with 8000x magnification; (c) image of MnS precipitation prills with 8000x magnification; (d) image of MnS precipitation dendrite with 5000x magnification.

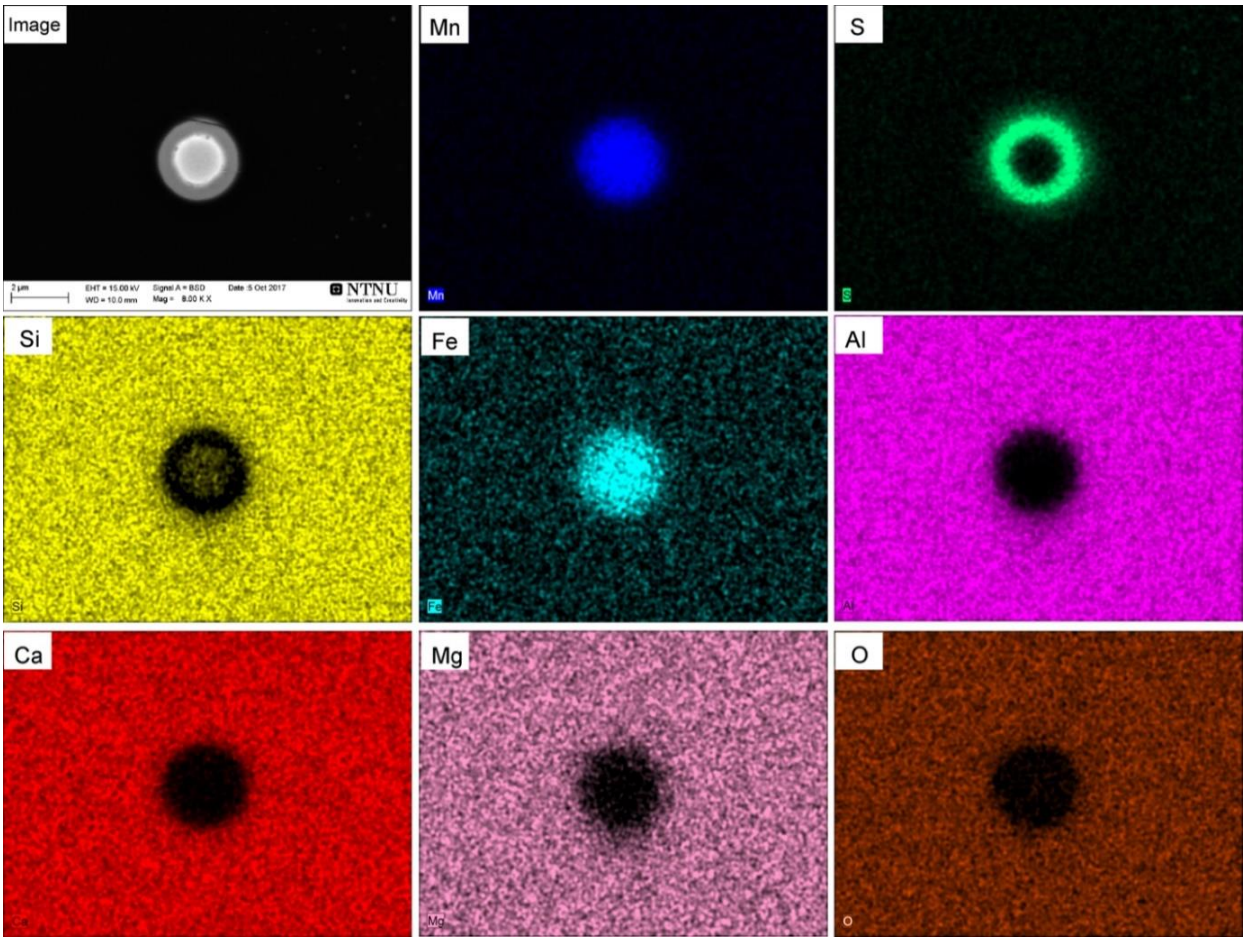

Fig. 9–EDS mapping results for Figure 8(b).

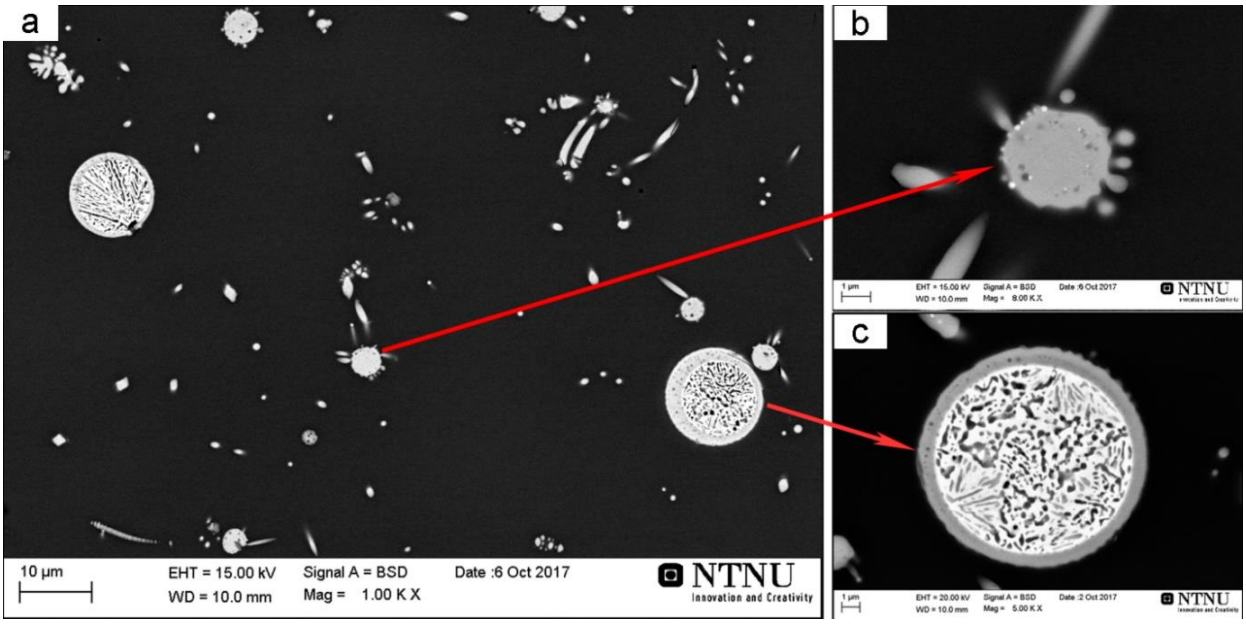

Fig. 10–The images of RM-4 slag after reduction. (a) Image with 1000x magnification; (b) image of MnS precipitation prills with 8000x magnification; (c) image of metal drop with MnS outer layer with 5000x magnification.

3.2 Wetting property of slag

The wetting property of slag on carbon black substrate is studied with a sessile drop furnace in the range of 1523 K to 1873 K (1250 °C to 1600 °C) at a heating rate of 10 K/min. The contact angle is the inner angle between the liquid-atmosphere interface and the liquid-solid interface. Figure 11 shows the change in the contact angle of different slags with temperature and time. The top right inset in Figure 11 shows the RM-3 slag on carbon black at 1873 K (1600 °C). As observed, carbon black is not wetted by the slag, and the contact angle is very high at all temperatures. For RM-1 slag, no significant change in the contact angle with the increase in temperature is observed, and the slag drop rolled off the substrate at 1827 K (1554 °C). The slag drop is easily moved on the substrate due to the poor wetting and gas generation on the slag-carbon interface. The sulphur-

287 containing slags reduce the contact angle with increasing temperature from 1523 K to 1873 K
288 (1250 °C to 1600 °C). The total changes in contact angle for RM-2, RM-3 and RM-4 are 4.5 °, 7.6
289 ° and 7.0 °, respectively. This finding may be due to the increasing wettability of the slag and
290 carbon black or/and the reduction of MnO. As shown in previous research results, the slag surface
291 tension decreases slightly with decreasing MnO content [27]. It is also noted that the contact angles
292 of slags with sulphur are all lower than RM-1, which indicates that sulphur may improve the
293 wetting property. However, connections between the sulphur content and slag contact angle on
294 carbon black are not observed.
295
296 The contact area of the slag drop with carbon black increases with decreased contact angle as
297 described by Eq. (10). The unit contact area is calculated by dividing the measured contact area by
298 the measured sessile volume and presented in Figure 12. The unit contact area of slags with sulphur
299 increases 79.6 pct to 93.1 pct compared to RM-1 slag at 1873 K (1600 °C). This contact area may
300 significantly accelerate the reaction rate between slag and carbon black.
301
302 $$S = \pi \cdot r^2 \cdot sin^2(180 - \theta) \quad (10)$$
303 where S is the contact area of the slag drop;
304 r is the radius of slag drop;
305 θ is the contact angle.
306

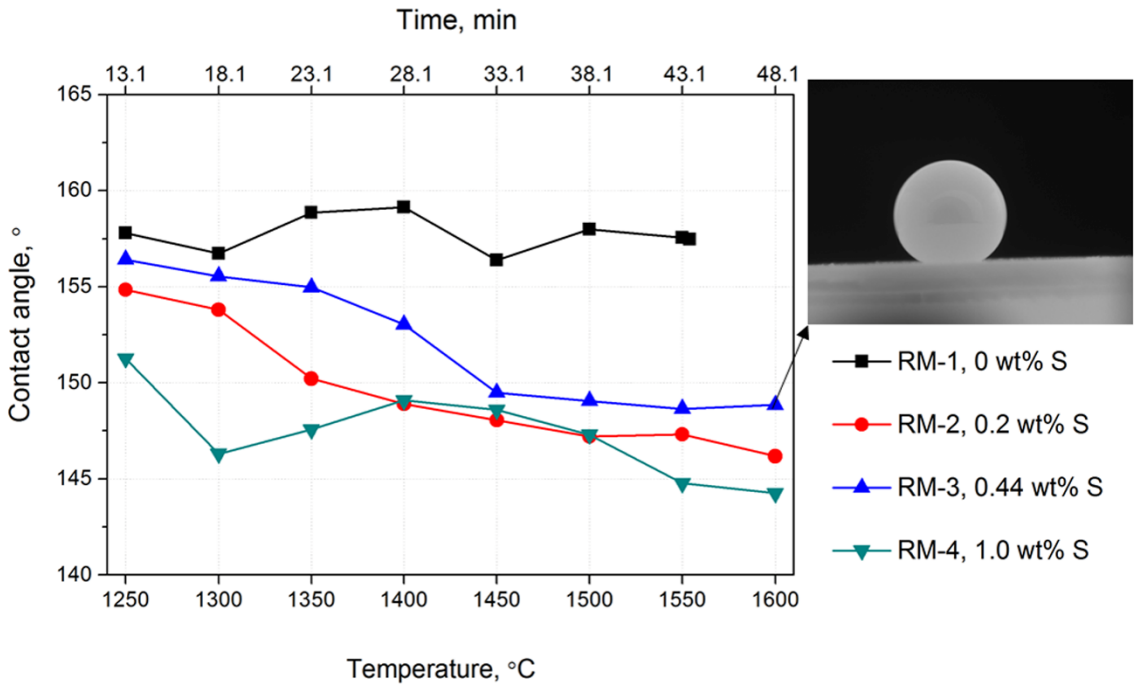

307

308 Fig. 11–The contact angles of slag with different sulphur contents on carbon black substrate versus

309 temperature and time.

310

311

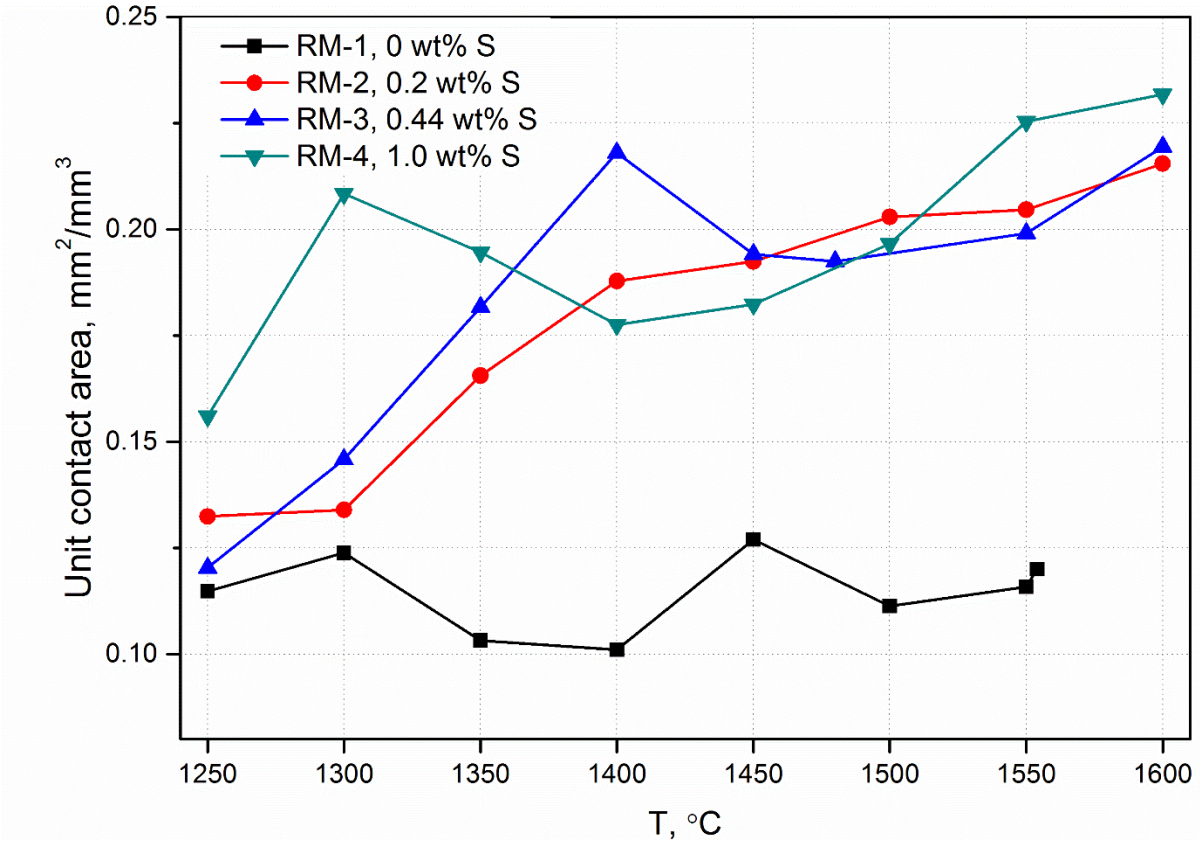

Fig. 12–The unit contact areas of slag with different sulphur contents on carbon black substrate versus temperature.

3.3 Slag-carbon and slag-metal interface reactivity

MnO and SiO_2 dissolved in slag are reduced to molten metal either by solid carbon or by carbon dissolved in metal. The former is defined as the slag-carbon interface reaction, and the latter is defined as the slag-metal interface reaction. The slag reduction described in Section 3.1 combines both slag-carbon and slag-metal interface reactions. Therefore, eight experiments are performed in the TG furnace at 1873 K (1600 °C) to study the effect of sulphur on slag-carbon and slag-metal interface reactivity, respectively. Carbon black is not used in these experiments because carbon

black will float on the surface of molten slag and make it difficult to calculate contact area. To study the interface reaction between slag and carbon, a graphite crucible and carbon black powder are considered the same.

The reduction curves of the four experiments are presented in Figure 13. The RM-1 slag-metal reaction rate is calculated directly from MC-1 TG curve. The weight loss over 30 min holding time is used to calculate the average reduction rate. The MC-2 TG curve is a combination of RM-1 slag-carbon and slag-metal reactions. Therefore, the RM-1 slag-carbon reaction rate is obtained by deducting the MC-1 reduction rate from the MC-2 reduction rate. The slag-metal and slag-carbon reaction rates of other slags are similarly calculated using their TG curves. The metallic prills are rare in the slag phase due to the relatively low reduction. Large amounts of metallic prills are not observed in the slag after reduction, similar to the morphologies shown in Figure 7. Therefore, the reaction between metallic prills and slag can be ignored.

The reactivity calculations are summarized in Table VI. The slag-carbon reaction surface area in experiments using a graphite crucible is 9.42 cm^2, and the estimated slag density is 3.1 g cm^{-3} assuming it remains constant during reduction [1]. The slag-carbon reaction surface area in experiments using a graphite crucible with Mo wall is zero. The slag-metal reaction surface area in all experiments is 7.07 cm^2 assuming that melted metal covers the bottom of the crucible. The slag-metal reaction rate constant ($k_{s\text{-}m}$) is one order higher than the slag-carbon reaction rate constant ($k_{s\text{-}c}$) for all slags. The $k_{s\text{-}m}$ is accelerated 2.2 times using RM-2 slag and accelerated 4.2 times using RM-3 slag. However, more sulphur (1.0 wt pct) reduces the $k_{s\text{-}m}$ to 3.9×10^{-3} g/min·cm^2.

The effect of sulphur on the $k_{s\text{-}c}$ is not obvious, possibly because the reaction rate between slag and C is low, and the calculation error cannot be ignored.

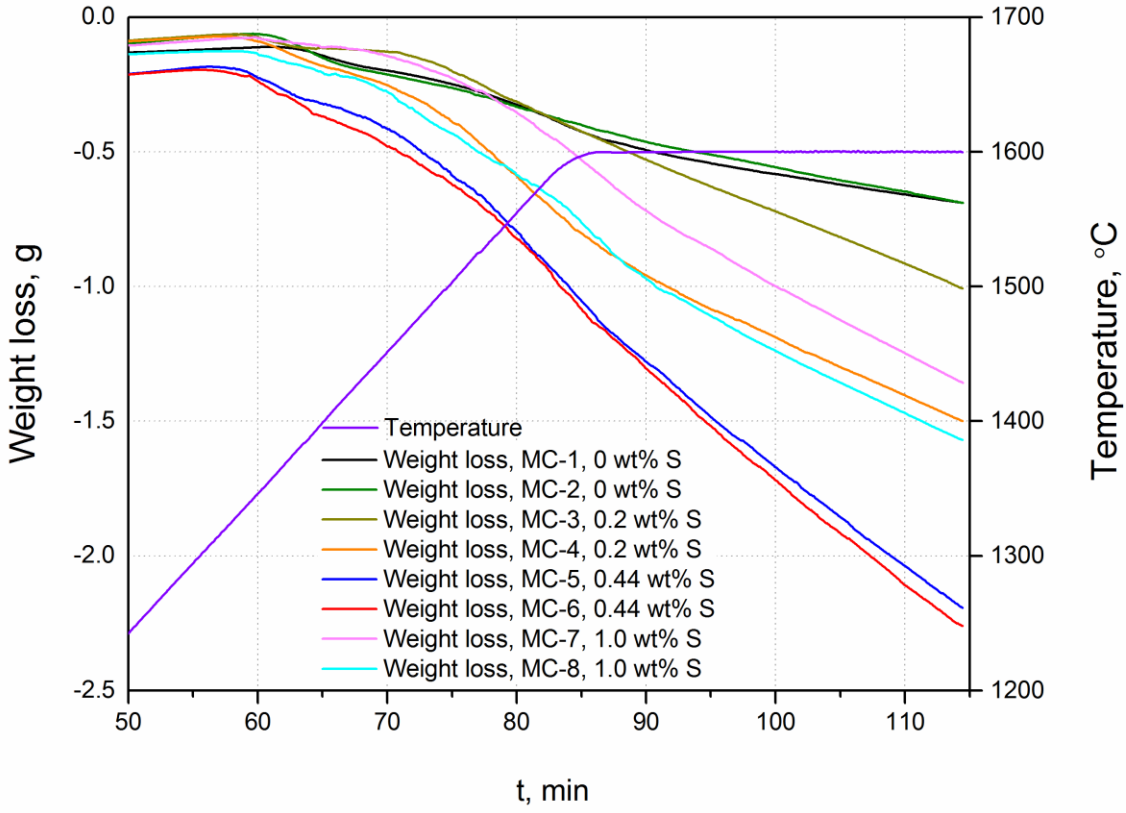

Fig. 13–Temperature profile and thermogravimetric curves for the experiments to determine the interface reaction rate.

Table VI. Interface reaction rate calculation results.

Interface reaction type	Slag used	Reaction rate ($g\ min^{-1}$)	Contact area (cm^2)	k ($g/min \cdot cm^2$)
slag-metal	RM-1	0.0092	7.07	1.3E-03
slag-metal	RM-2	0.0198	7.07	2.8E-03
slag-metal	RM-3	0.0389	7.07	5.5E-03
slag-metal	RM-4	0.0276	7.07	3.9E-03
slag-carbon	RM-1	0.0007	9.42	7.4E-05
slag-carbon	RM-2	0.0039	9.42	4.2E-04
slag-carbon	RM-3	0.0012	9.42	1.3E-04
slag-carbon	RM-4	0.0005	9.42	5.7E-05

4. Discussion

4.1 MnS precipitation process

A large amount of MnS precipitation is observed in RM-3 and RM-4 slag after reduction (Figure 8 and 10) but not in RM-2 slag (Figure 7). Whether the precipitation process occurs during reduction at 1873 K (1600 °C) or during slag cooling is very important. Therefore, ternary phase diagrams of MnS-MnO-SiO_2-Al_2O_3 (with fixed SiO_2/Al_2O_3=1.8) at different temperatures are calculated by Factsage 7.0 with "FTmisc" and "FToxid" databases. Figure 14 shows the phase diagrams of the above system at 1873 K (1600 °C), where the reduction paths of RM-3 and RM-4 are also marked. It is clear that in the isothermal stage at 1873 K (1600 °C), RM-3 and RM-4 do not enter into the MnS precipitation zone due to the low MnS wt pct.

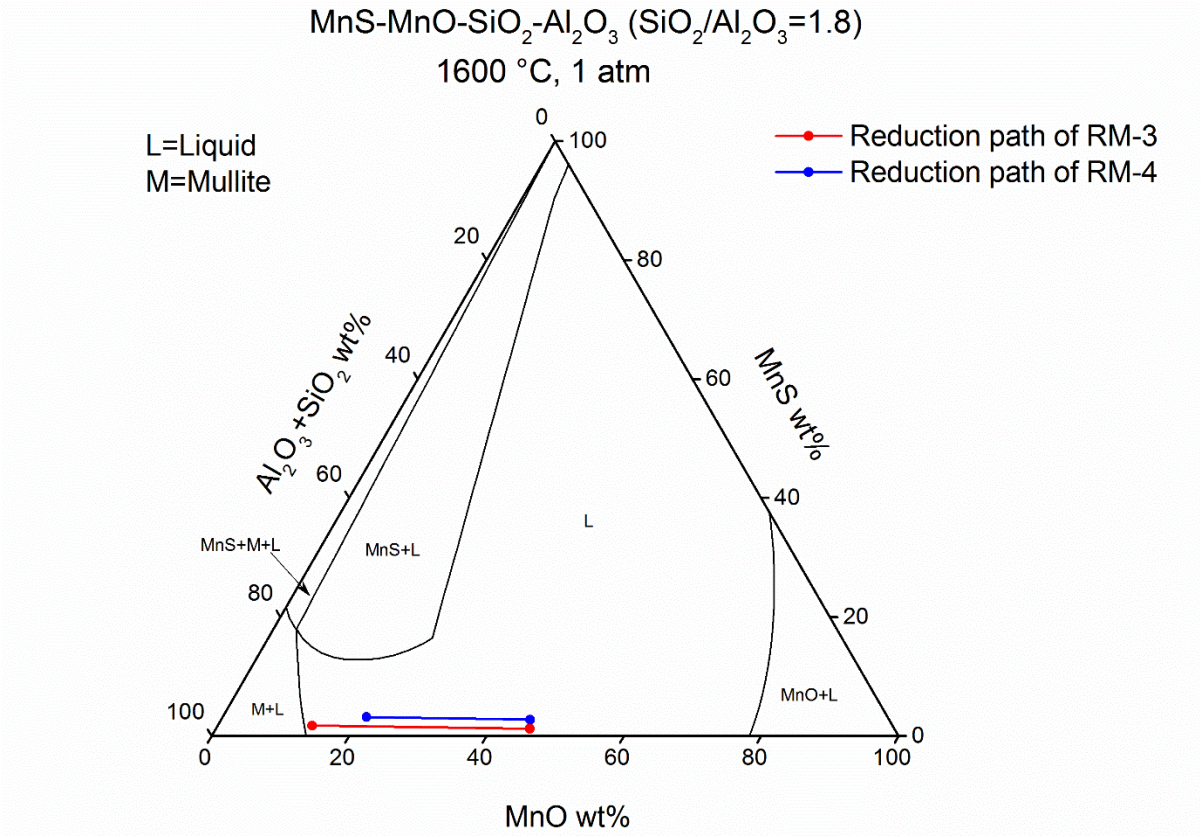

370

371 Fig. 14–Calculated phase diagram of the MnS-MnO-SiO_2-Al_2O_3 (SiO_2/Al_2O_3=1.8) system at 1873

372 K (1600 °C), and the reduction paths of RM-3 and RM-4 are indicated.

373

374 The effect of temperature on the MnS precipitation zone is presented in Figure 15. The MnS

375 precipitation zone expands with the cooling process from 1873 K to 1473 K (1600 °C to 1200 °C),

376 and the precipitation line is closer to the bottom of the ternary phase diagrams. For a given slag

377 composition, lower temperature is favourable for MnS precipitation.

378

379 Figure 16 shows the effect of MnO content on the MnS precipitation line, where the data form

380 Figure 17, and the MnS wt pct is converted to S wt pct. In the temperature range of 1473 K to 1773

381 K (1200 °C to 1500 °C), for a given sulphur content in the slag, lower MnO content is favourable

for MnS precipitation. At 1873 K (1600 °C), MnS precipitation only occurs when the sulphur content is higher than 4.71 wt pct, which far exceeds sulphur content in industrial slags [17]. At 1473 K (1200 °C), the sulphur content at the MnS precipitation point dropped from 1.29 to 0.12 wt pct when MnO content decreased from 40 to 5 wt pct. This drop indicates that the reduction process promotes MnS precipitation during slag cooling.

As the liquidus temperature of SiMn slag is below 1573 K (1300 °C) [1], the phase diagram at 1473 K (1200 °C) is used to describe the final slag phase after cooling. The partially enlarged phase diagram of the MnS-MnO-SiO_2-Al_2O_3 (SiO_2/Al_2O_3=1.8) system at 1473 K (1200 °C) is shown in Figure 17. The slag compositions of 10 experimental points are marked as red spots. The conditions and results for the 10 experimental points are listed in Table VII. For RM-3 and RM-4 slag, experiments stopped at different holding times at 1873 K (1600 °C). The slag collected from Experiments a, b, c, f and g, i.e., the red spots below the line, do not contain MnS precipitation in their SEM images. For the spots above the line, MnS precipitation is observed in the corresponding slag images. SEM images of d, h and j slag containing MnS precipitation are also shown in Figure 17. SEM images of e and k slag are previously presented in Figure 8 and 10, respectively. The experiment results fit well with the calculation phase diagram.

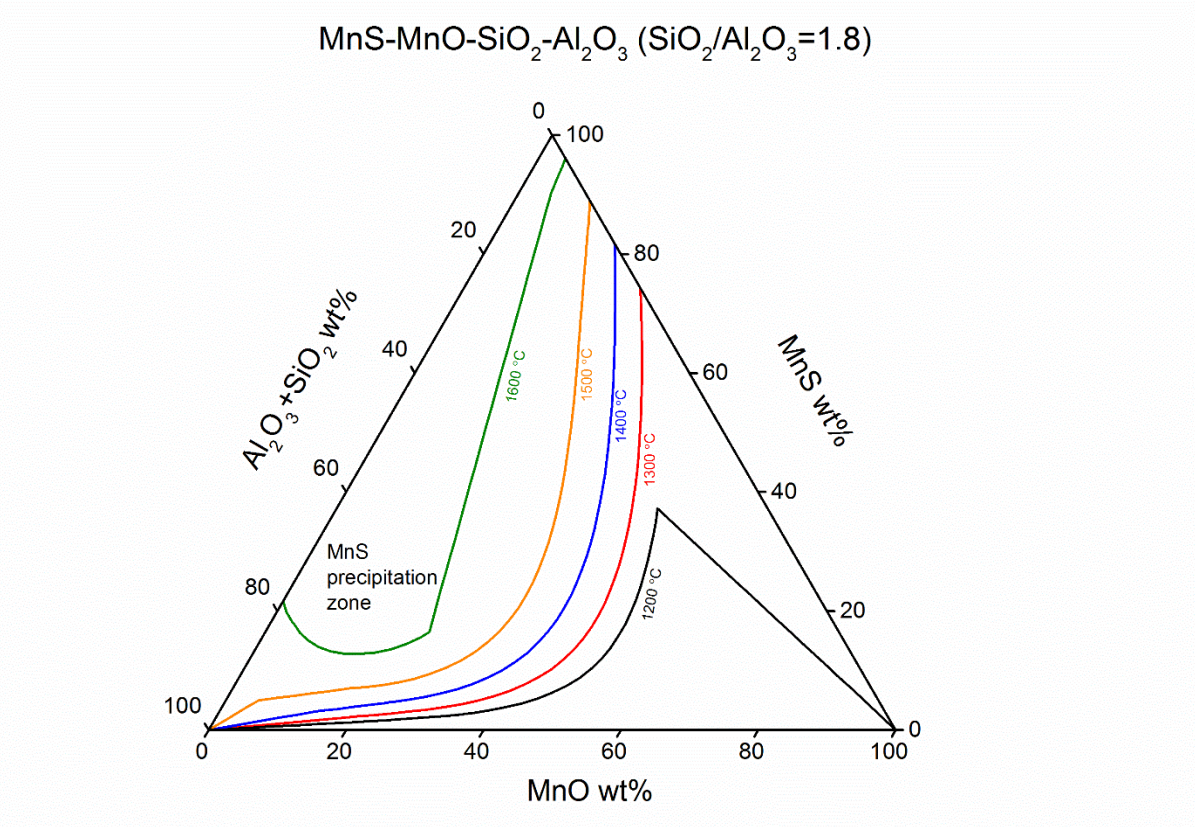

400

401 Fig. 15–The effect of temperature on the MnS precipitation zone.

402

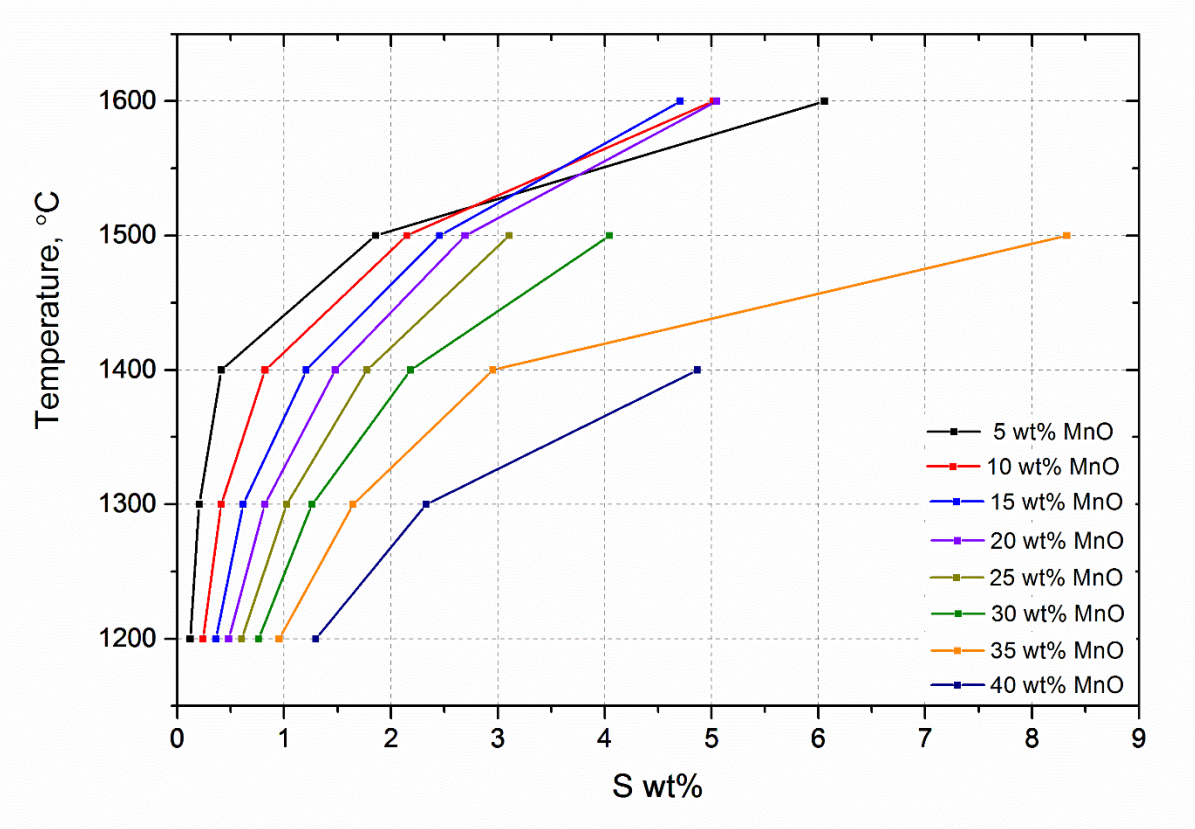

403

404 Fig. 16–The effect of MnO content on the MnS precipitation line.

405

406

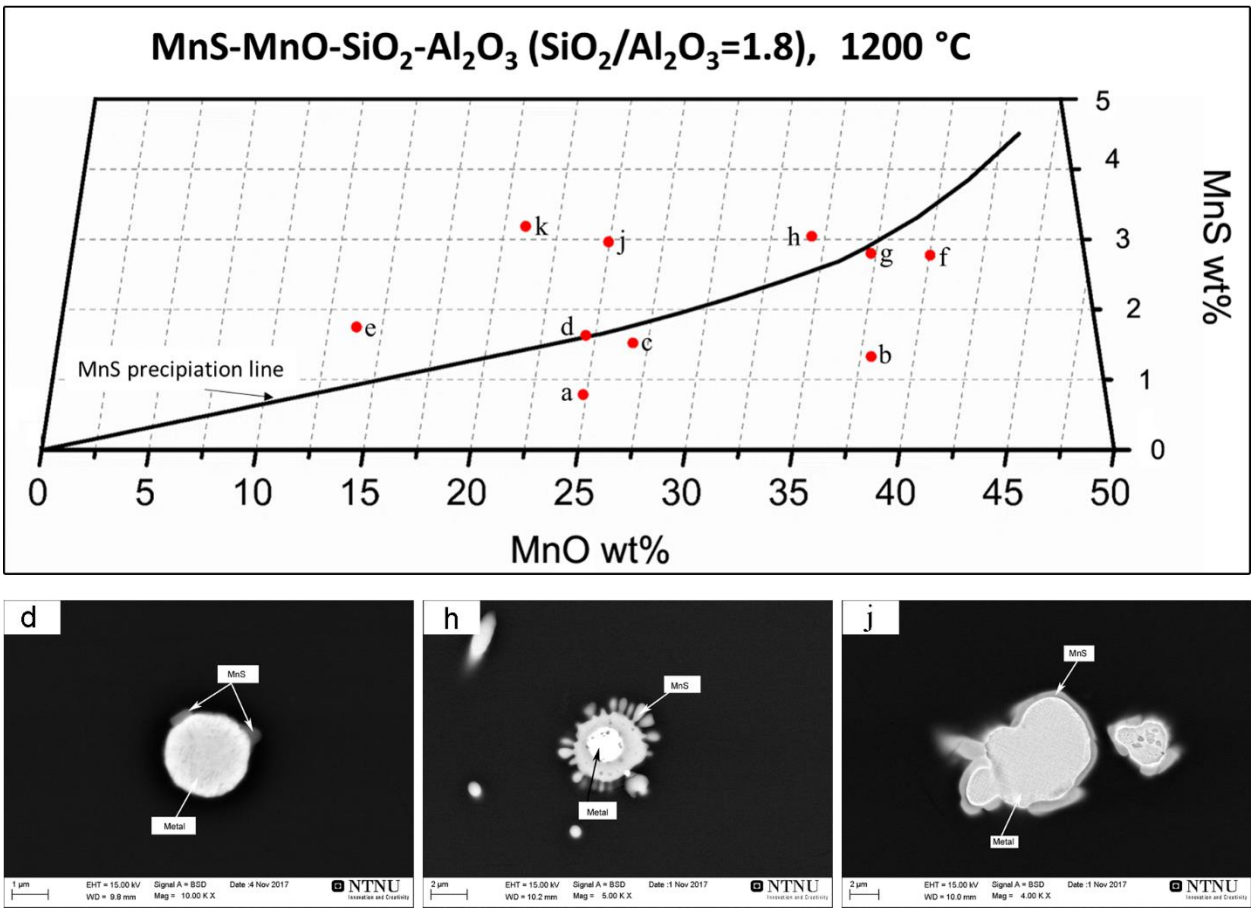

Fig. 17–Partially enlarged phase diagram of the MnS-MnO-SiO_2-Al_2O_3 (SiO_2/Al_2O_3=1.8) system at 1473 K (1200 °C). The red spots show the slag composition of experimental points. The images of slag after reduction for experiments d, h and j are inserted.

Table VII. The conditions and results for experimental points indicated in Figure 17.

Experimental point	1873 K holding time (min)	Slag type	Measured S content (wt pct)	Calculated MnS content (wt pct) *	Normalized MnO content (wt pct) §	MnS precipitation
A	60	RM-2	0.29	0.79	24.9	No
B	20	RM-3	0.49	1.33	38.0	No
C	40	RM-3	0.56	1.52	26.8	No
D	50	RM-3	0.60	1.63	24.6	Yes
E	60	RM-3	0.64	1.75	13.8	Yes
F	20	RM-4	1.02	2.77	40.0	No
G	30	RM-4	1.03	2.80	37.3	No
H	40	RM-4	1.12	3.05	34.4	Yes
J	50	RM-4	1.09	2.96	25.0	Yes
K	60	RM-4	1.17	3.18	21.0	Yes

$* \; Calculated\ MnS\ wt\ pct = \frac{S\ wt\ pct}{32} \times 87$

$\S \; Normalized\ MnO\ pct = \frac{MnO\ pct}{MnS\ pct + MnO\ pct + SiO_2\ pct + Al_2O_3\ pct} \times 100$

4.2 Reduction kinetics

Previous studies have shown that the reduction rate of MnO can be described by Eq. (11) [1, 28]. Assuming that the SiO_2 reduction in the SiMn slag system is also controlled by chemical reaction, a similar kinetic model for SiO_2 reduction can be modelled with Eq. (12) [22, 25].

$$R_{MnO} = k_{Mn} \cdot A \cdot \left(a_{MnO} - \frac{a_{Mn} \cdot p_{CO}}{K_{T,Mn}}\right)$$

$$= \underbrace{k_{0,Mn}\, exp(-E_{MnO}/RT)}_{rate\ constant} \cdot \underbrace{A_c}_{contact\ area} \cdot \underbrace{(a_{MnO} - a_{Mn} p_{CO}/K_{T,Mn})}_{driving\ force} \qquad (11)$$

$$R_{SiO_2} = k \cdot A \cdot \left(a_{SiO_2} - \frac{a_{Si} \cdot p_{CO}^2}{K_{T,Si}}\right)$$

$$= \underbrace{k_{0,Si}\, exp\left(-E_{SiO_2}/RT\right)}_{rate\ constant} \cdot \underbrace{A_c}_{contact\ area} \cdot \underbrace{\left(a_{SiO_2} - a_{Si} p_{CO}^2 / K_{T,Si}\right)}_{driving\ force} \quad (12)$$

where R is the reduction rate (g/min), k is the rate constant (g/min·cm^2), k_o is the frequency factor, A_c is the interfacial area (cm^2), E is the activation energy (kJ/mol), R is the gas constant, T is the temperature, a_{MnO} and a_{SiO_2} are the activities of MnO and SiO_2 in the slag phase, a_{Mn} and a_{Si} are the activities of Mn and Si in the metal phase, p_{CO} is the partial pressure of CO(g) and K_T is the equilibrium constant at temperature T.

The reduction rate as a function of time is calculated by the differential of the weight loss curves as shown in Figure 18. The driving forces for MnO and SiO_2 reduction versus time are calculated in the increasing temperature stage (every other 50 K from 1573 K to 1873 K (1300 °C to 1600 °C)) and the isothermal stage (every 10 min) and presented in Figure 19. Slag composition at each point is calculated based on the weight loss data shown in Figure 5 and assuming that both MnO and SiO_2 reduction contributes 50 pct to the weight loss. It is worth pointing out that the contribution of SiO_2 reduction is less than 50 pct in actual performance. It is calculated to be 38.2 pct, 40.4 pct, 45.2 pct and 44.6 pct for RM-1, RM-2, RM-3 and RM-4, respectively, based on the final slag compositions shown in Table IV. While the number at each point is assumed to be 50 % for greatly reducing the number of experiments, it does not affect the trend of the driving force of MnO and SiO_2. a_{MnO}, a_{SiO_2}, a_{Mn}, and a_{Si} are calculated by Eq. (3), Eq. (4), Eq. (5) and Eq. (6), respectively. All slags show an increasing trend for the MnO driving force with the increase in temperature and follow a decreasing trend in the isothermal stage due to the drop in MnO activity in slag with reduction. In the RM-3 slag, the driving force decreases fastest due to having the

highest reduction rate. For the SiO_2 reduction, all slags show an almost invariable driving force during the reduction process, and their driving forces are close to each other except the dot of RM-1 at 1573 K (1300 °C). The reason may be that SiO_2 content changes slightly during reduction, as shown in Table IV.

The reported activation energy for the carbothermal reduction of MnO ranges from 332 to 407 kJ/mol [7, 8, 28, 29], and for the carbothermal reduction of SiO_2, the range is 796–870 kJ/mol [22, 25, 30]. Therefore, the reduction of MnO and SiO_2 is highly sensitive to temperature. The RM-1 reduction rate curve in Figure 18 shows a unimodal curve. The reduction rate of RM-1 increases with the increase in temperature and reaches a peak at 1873 K (1600 °C), then decreases rapidly with the extension of holding time and increased reduction. In the increasing temperature stage, the rate constant increases dramatically with the increase in temperature, the contact area remains constant, the driving force for MnO increases from 0.10 to 0.17, and the driving force for SiO_2 increases from 0.09 to 0.12. The RM-1 slag reduction curve in the isothermal stage is quite similar to a previous study of MnO reduction curves [5, 7, 31], in which the reduction rate drops rapidly due to the decrease in driving force in the homogenous liquid slag.

In Figure 18, slags with sulphur show similar reduction curves to RM-1 in the increasing temperature stage. They show, however, different curves in the isothermal temperature stage. Their reduction rates do not decrease with the decrease in slag activity but increases to higher levels. Among them, RM-3 slag shows a significantly higher reduction rate compared to RM-1 slag.

In the increasing temperature stage, the metal produced in the system is low. Therefore, the slag-carbon interface reaction dominates slag reduction in this stage. Although the contact area between carbon black and slag with sulphur is significantly higher, as described in Figure 12, the effect of sulphur on slag-carbon reaction rate constant ($k_{s\text{-}c}$) is unconfirmed as described in Table VI.

In the isothermal stage, with the increased amount of metal produced, the contact area between slag and metal keeps increasing. The other fact is that $k_{s\text{-}m}$ is much higher than $k_{s\text{-}c}$. Therefore, the slag-metal interface reaction becomes increasingly important. Sulphur is confirmed to produce greater acceleration on the $k_{s\text{-}m}$. This increased acceleration may explain the reduction curves of slag with sulphur in the isothermal stage.

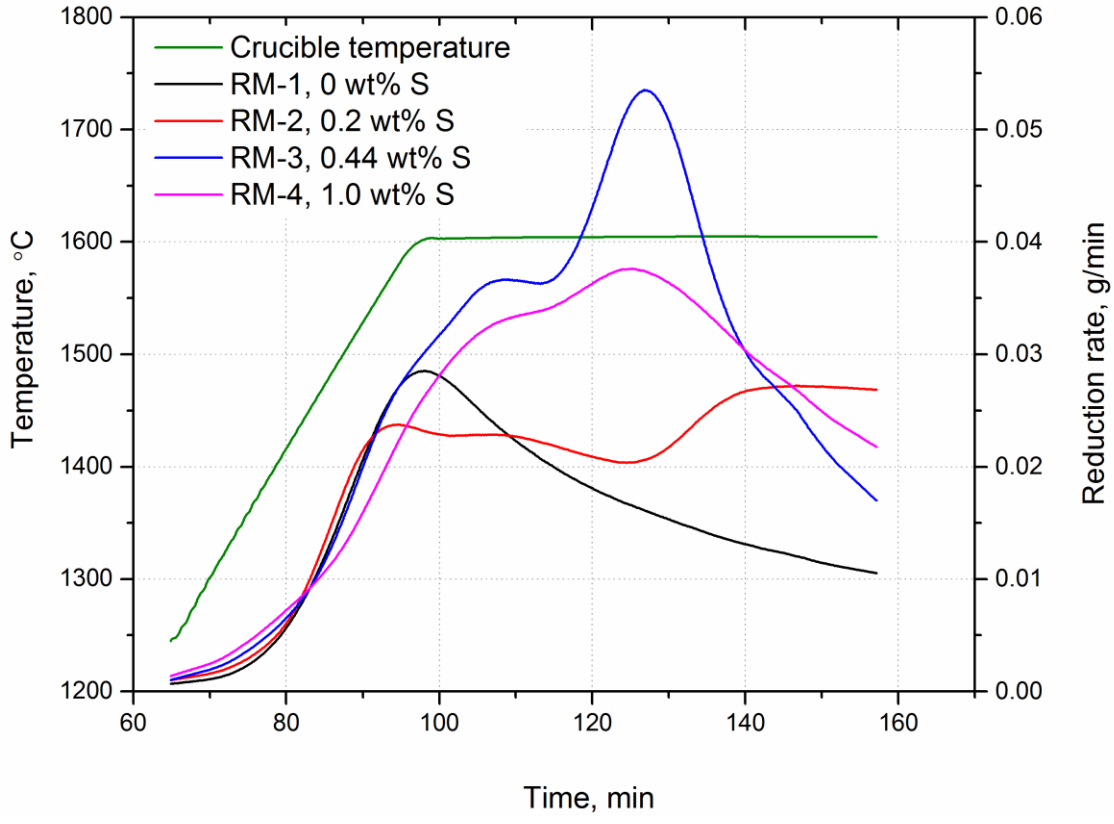

Fig. 18–Calculated reduction rate versus time.

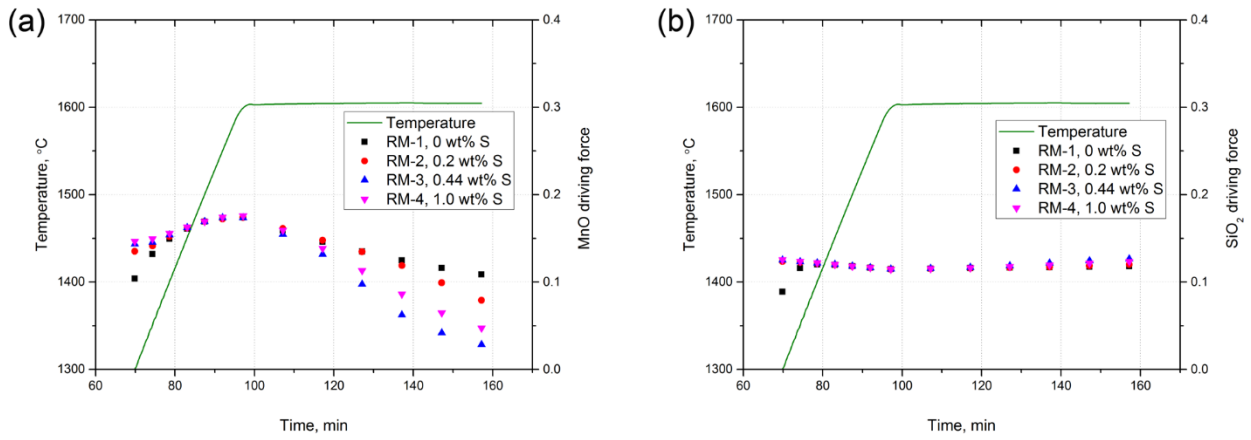

Fig. 19–Calculated driving forces for MnO (a) and SiO_2 (b) reduction versus time.

5. Conclusions

The reduction of SiMn slags with different sulphur contents is studied at 1873 K (1600 °C) under CO atmospheric pressure. Sulphur does not have an obvious effect on the contact angle of slag on carbon black, with sulphur content varying from 0.2 wt pct to 1.0 wt pct. However, the unit contact area increases significantly for the slag with sulphur. It is confirmed that small amounts of sulphur in slag significantly improve the reduction of MnO and SiO_2. The reaction rate on the slag-metal interface is much higher than on the slag-carbon interface, and sulphur has greater acceleration on the former interface.

MnS precipitation is generated in RM-3 and RM-4 slag during slag cooling. For a given slag composition, lower temperature and higher sulphur content are favourable for MnS precipitation. For a given sulphur content and temperature, lower MnO content is favourable for MnS precipitation.

Acknowledgements

This research is supported under the Norwegian Research Council (GasFerroSil, project No. 224950). The authors would also like to thank Dr. Kai Tang from SINTEF Materials and Chemistry for his assistance with thermodynamic calculations.

References

1. S.E. Olsen, M. Tangstad and T. Lindstad: *Production of Manganese Ferroalloys*, Tapir Academic Press, Trondheim, Norway, 2007.

2. O. Ostrovski and D. Swinbourne: *Steel. Res. Int.*, 2013, vol. 84, pp. 680–6.

3. T. Coetsee, C. Reinke, J. Nell and P.C. Pistorius: *Metall. Mater. Trans. B*, 2015, vol. 46, pp. 2534–52.

4. J.H. Stansbie: *Iron and Steel*, Read Books, Worcestershire, UK, 2007, pp. 351–2.

5. M. Tangstad: *The High Carbon Ferromanganese Process–Coke Bed Relations*, PhD Thesis, Norwegian Institute of Technology, Trondheim, Norway, 1996.

6. K. Xu, G. Jiang, W. Ding, L. Gu, S. Guo and B. Zhao: I*SIJ Int.*, 1993, vol. 33, pp. 104–8.

7. J. Safarian and L. Kolbeinsen: *Metall. Mater. Trans. B*, 2015, vol. 46: 125–34.

8. T.A. Skjervheim: *Kinetics and mechanisms for transfer of manganese and silicon from melten oxide to liquid manganese metal*, PhD Thesis, Norwegian Institute of Technology, Trondheim, Norway, 1994.

9. J.F. White, J. Lee, O. Hessling and B. Glaser: *Metall. Mater. Trans. B*, 2017, vol. 48: 506–15.

10. J.F. White, J. Lee, O. Hessling and B. Glaser: *Proceedings of the 10th International Conference on Molten Slags, Fluxes and Salts*, Seattle, USA, 2016, pp. 565–72.

11. H. Sun, K. Mori and R.D. Pehlke: *Metall. Trans. B*, 1993, vol. 24, pp. 113–20.

12. I. Egry, E. Ricci, R. Novakovic and S. Ozawa: *Adv. Colloid. Interfac.*, 2010, vol. 159, pp. 198–212.

13. T. Dubberstein, H. Heller, J. Klostermann, R. Schwarze and J. Brillo: *J. Mater. Sci.*, 2015, vol. 50, pp. 7227–37.

14. T. Dubberstein, A. Jahn, M. Lange, H. Heller and P.R. Scheller: *Steel. Res. Int.*, 2014, vol. 85, pp. 1220–8.

15. T. Zienert, S. Dudczig, O. Fabrichnaya and C.G. Aneziris: *Ceram. Int.*, 2015, vol. 41, pp. 2089–98.

16. K. Xu, W. Ding and G. Jiang: *Shenyang International Symposium on Smelting Reduction*, Shengyan, China, 1986, pp. 191–206.

17. T.A. Skjervheim and S.E. Olsen: *Proceedings of the 7th International Congress on Ferroalloys (INFACON VII)*, Trondheim, Norway, 1995, pp. 631–40.

18. T.A. Larssen: *Reduction of MnO and SiO_2 from Assmang and Comilog based Slags*, Master's thesis, Norwegian University of Science & Technology, Trondheim, Norway, 2017.

19. P.P. Kim, M. Tangstad: *Metall. Mater. Trans. B*, 2018, vol. 49, pp. 1185–1196.

20. R. Kawamoto: *Effect of Sulphur addition on the reduction mechanism of synthetic siliconmanganese ore*, Norwegian University of Science & Technology Report, 2017.

21. M.M. Yastreboff: *Mechanisms of Carbothermic Reduction of Manganese Oxide from Manganese Ore and Ferromanganese Slag*, PhD Thesis, The University of New South Wales, Sydney, Australia, 2000, pp. 170–2.

22. P. Kim, T.A. Larssen, M. Tangstad and R. Kawamoto: *Applications of Process Engineering Principles in Materials Processing, Energy and Environmental Technologies, Part of the series The Minerals, Metals & Materials Series*, San Diego, USA, 2017, pp. 475–83.

23. J. Safarian, G. Tranell, L. Kolbeinsen, M. Tangstad, S. Gaal and J. Kaczorowski: *Metall. Mater. Trans. B*, 2008, vol. 39, pp. 702–12.

24. Y. Park and D.J. Min: *ISIJ Int.*, 2016, vol. 56, pp. 520–6.

25. J.S. Oh and J. Lee: *J. Mater. Sci.*, 2016, vol. 51, pp. 1813–9.

26. C.W. Bale, E. Bélisle, P. Chartrand, S.A. Decterov, G. Eriksson, A.E. Gheribi, K. Hack, I-H. Jung, Y-B. Kang, J. Melançon, A.D. Pelton, S. Petersen, C. Robelin, J. Sangster, P. Spencer and M-A. Van Ende: *Calphad J.*, 2016, vol. 55, pp. 1–19.

27. O. Ostrovski, S.E. Olsen, M. Tangstad and M. Yastreboff: *Can. Metall. Quart.*, 2002, vol. 41, pp. 309–18.

28. H. Olsen: *A Theoretical Study on the Reaction Rates in the SiMn Production Process, Master's thesis*, Norwegian University of Science & Technology, Trondheim, Norway, 2016.

29. T. Shimoo, S. Ando and H. Kimura: *J. Jpn. I. Met.*, 1984, vol. 48, pp. 922–9.

30. A. Blackman and L. Gahan: *Aylward and Findlay's SI Chemical Data*, 7th Edition, Wiley, New Jersey, USA, 2014.

31. M. Yastreboff, O. Ostrovski and S. Ganguly: *ISIJ Int.*, 2003, vol.43, pp. 161–5.

572 **List of Tables**

573

582

583

584

585 **Figure Captions**

586

587 Fig. 1–The images of synthetic slags RM-1, RM-2, RM-3 and RM-4 taken during EDS mapping.

588 Fig. 2–Schematics of the thermo-gravimetric (TG) furnace, reprinted from Ref. [22].

589 Fig. 3–Sessile drop experimental setup, reprinted from Ref. [23].

590 Fig. 4–The schematic view of the experimental setup for slag-carbon and slag-metal interface
591 reaction rate testing.

592 Fig. 5–Temperature profile and thermogravimetric curves for experiments with different sulphur
593 contents in slag using carbon black as the reductant.

594 Fig. 6–The image of metal phase of RM-3 after reduction.

595 Fig. 7–The images of RM-1 and RM-2 slag after reduction.

596 Fig. 8–The images of RM-3 slag after reduction. (a) Image with 1000x magnification; (b) image
597 of metal drop with MnS outer layer with 8000x magnification; (c) image of MnS
598 precipitation prills with 8000x magnification; (d) image of MnS precipitation dendrite with
599 5000x magnification.

600 Fig. 9–EDS mapping results for Figure 8(b)

601 Fig. 10–The images of RM-4 slag after reduction. (a) Image with 1000x magnification; (b) image
602 of MnS precipitation prills with 8000x magnification; (c) image of metal drop with MnS
603 outer layer with 5000x magnification.

604 Fig. 11–The contact angles of slag with different sulphur contents on carbon black substrate versus
605 temperature and time.

606 Fig. 12–The unit contact areas of slag with different sulphur contents on carbon black substrate
607 versus temperature.

608 Fig. 13–Temperature profile and thermogravimetric curves for the experiments to determine the
609 interface reaction rate.
610 Fig. 14–Calculated phase diagram of the MnS-MnO-SiO_2-Al_2O_3 (SiO_2/Al_2O_3=1.8) system at 1873
611 K (1600 °C), and the reduction paths of RM-3 and RM-4 are indicated.
612 Fig. 15–The effect of temperature on the MnS precipitation zone.
613 Fig. 16–The effect of MnO content on the MnS precipitation line.
614 Fig. 17–Partially enlarged phase diagram of the MnS-MnO-SiO_2-Al_2O_3 (SiO_2/Al_2O_3=1.8) system
615 at 1473 K (1200 °C). The red spots show the slag composition of experimental points.
616 The images of slag after reduction for experiments d, h and j are inserted.
617 Fig. 18–Calculated reduction rate versus time.
618 Fig. 19–Calculated driving forces for MnO (a) and SiO_2 (b) reduction versus time.
619